


FULL PAPER

Open Access



Anisotropic structure at shallow depths across the Japan Trench

Takashi Tonegawa^{1*} , Katsuhiko Shiomi² and Ryota Takagi³

Abstract

Anisotropic structures within the crust are frequently perceived to originate from stress-induced cracks, which have been mainly estimated on land through different wave speeds of orthogonally polarized S waves propagating in the anisotropic media. However, such estimations of crustal anisotropic structures in ocean areas, particularly for subduction zones around trenches, have not been investigated in detail due to the lack of long-term ocean bottom observations. In this study, we used ocean bottom seismometers of a permanent network deployed across the Japan Trench and the southern part of the Kuril Trench and applied the shear-wave splitting analysis to P-to-s converted waves extracted by receiver function analyses using teleseismic events. We estimated the anisotropic structures in marine sediments and oceanic crust for the incoming Pacific Plate and marine sediments for the overriding North American Plate. The obtained fast polarization directions for the incoming plate are mainly oriented to be parallel to the trench axis for the marine sediment and oceanic crust, which are formed by normal faults and cracks due to the upward plate bending in the outer-rise region, whereas results for marine sediments at the northern part of the Japan Trench are obliquely aligned to the trench axis. The oblique direction is consistent with the magnetic lineations of the incoming plate, indicating that ancient faults within the plate, which were formed in the shallow part of the crust during the creation of the oceanic plate at the ridge, are reactivated by the plate flexure. For the overriding plate, the fast polarization directions in the northern and southern parts of the study area are nearly normal to the trench axis. The central part shows two distinct features: the fast polarization directions parallel to the trench axis and small degrees of anisotropy. These patterns may reflect crack alignments associated with the lateral variation in postseismic crustal deformation after the 2011 Tohoku-Oki earthquake. Our results suggest substantial lateral variations in the stress field at the tip of the overriding plate along the strike direction.

Keywords S-wave splitting, Anisotropy, Marine sediment, Oceanic crust, Receiver function, Japan Trench

*Correspondence:

Takashi Tonegawa

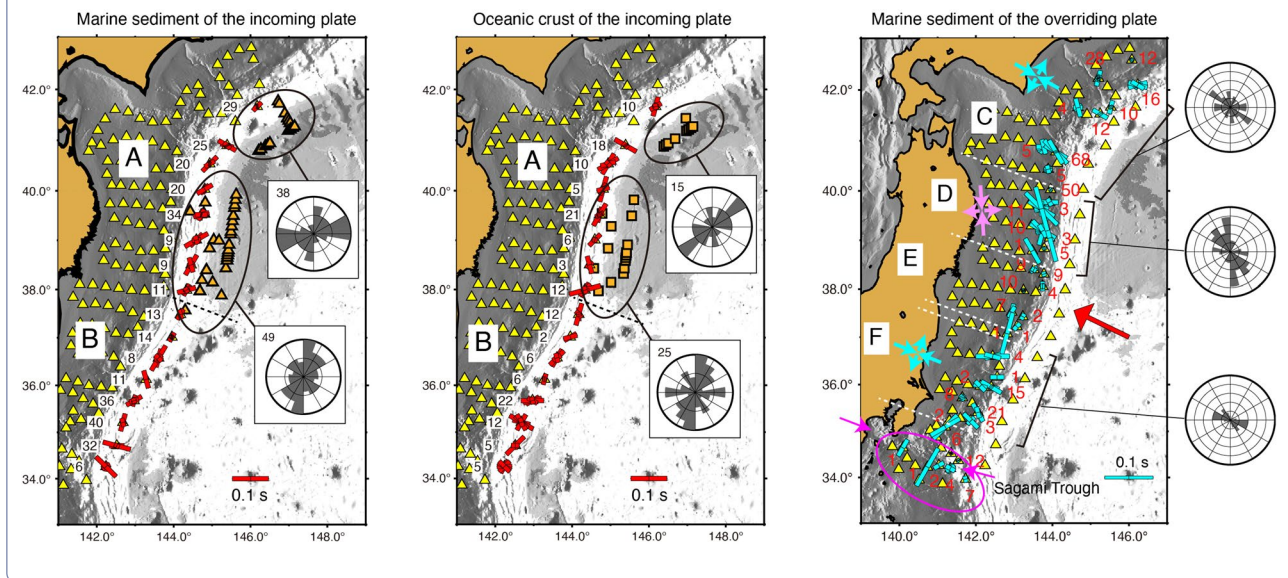
tonegawa@jamstec.go.jp

Full list of author information is available at the end of the article



© The Author(s) 2024. **Open Access** This article is licensed under a Creative Commons Attribution 4.0 International License, which permits use, sharing, adaptation, distribution and reproduction in any medium or format, as long as you give appropriate credit to the original author(s) and the source, provide a link to the Creative Commons licence, and indicate if changes were made. The images or other third party material in this article are included in the article's Creative Commons licence, unless indicated otherwise in a credit line to the material. If material is not included in the article's Creative Commons licence and your intended use is not permitted by statutory regulation or exceeds the permitted use, you will need to obtain permission directly from the copyright holder. To view a copy of this licence, visit <http://creativecommons.org/licenses/by/4.0/>.

Graphical Abstract



1 Introduction

Applying the deviatoric stress to the crust produces alignments of the cracks. The existence of these fracture lineations can be investigated through the seismological anisotropic structure. The anisotropic structure is estimated by splitting analyses, because seismic waves in anisotropic media have different propagation velocities in response to their polarization directions (e.g., Crampin 1977, 1981). In subduction zones, the incoming plates subduct underneath the overlying plates, producing stress fields within the overriding plates. Their status fluctuates spatio-temporally due to other factors, particularly for crustal deformations due to earthquakes and slow slips near the plate boundary. This indicates that the estimation of anisotropic structures in subduction zones contributes to understanding the current status of the stress field within the crust.

The Pacific Plate subducts beneath the North American Plate from the Japan and Kuril Trenches, and large earthquakes infrequently occur at the plate interface, inducing crustal deformations in the overriding plates (e.g., Ito et al. 2011; Dhar et al. 2023; Shibazaki 2023). A permanent network of ocean bottom seismometers has been deployed around the Japan Trench since September 2016 (S-net: the Seafloor Observation Network for Earthquakes and Tsunamis) (Aoi et al. 2020), and various characteristics of the observed recordings have been analyzed (e.g., Sawazaki et al. 2020; Dhakal et al. 2023; Tonegawa et al. 2023). The seismic anisotropy has been investigated by applying S-wave splitting analyses to recordings

obtained by the S-net (Uchida et al. 2020). However, its survey is mainly conducted in landward areas of the S-net due to the lack of interplate earthquakes near the trench and also the obtained anisotropic parameters reflect S-wave splitting along the entire ray paths. In this study, we apply receiver function (RF) analyses (Langston 1979; Ammon 1991) to teleseismic P-wave codas acquired by S-net stations west of the Japan Trench, and explore the anisotropic structure of marine sediments near the trench, which enables us to obtain layered anisotropic parameters and decipher the stress field at the tip of the overlying plate. Although an RF study using S-net data imaged the dipping discontinuities associated with the Pacific Plate at depth (Kim et al. 2021), our study focuses on seismic velocity discontinuities and anisotropic structures at shallow depths.

Moreover, the S-net contains stations deployed east of the Japan Trench. We also apply RF analyses to the recordings from the stations, which allows us to investigate the anisotropic structure within the incoming plate. The anisotropic structures of marine sediments in the Pacific Plate have been revealed by ambient noise analyses (Tonegawa et al. 2013, 2015), and those in marine sediments and igneous oceanic crust have been unveiled from P-to-s converted waves (Tonegawa et al. 2018). However, their survey areas are mainly in the outer-rise region where the plate is distorted upward due to plate subduction. Because the S-net stations are installed near the trench, we can investigate the anisotropic structure at the top part of the incoming plate before the subduction,

as well as their lateral variations in the seaward outer-rise region by comparing our results with those of previous studies. Moreover, the investigation of the lateral variations in the anisotropic structure across the Japan Trench contributes to the understanding of the stress fields in the overlying and incoming plates and their spatial continuity.

2 Data

The S-net consists of 150 seismic stations connected to 6 submarine cables (Fig. 1). Teleseismic P waves recorded at stations with water depths shallower than 2,500 m are overlapped with their water reverberations and are not used for the receiver function analysis in this study, which will be discussed later. Therefore, we examine 50

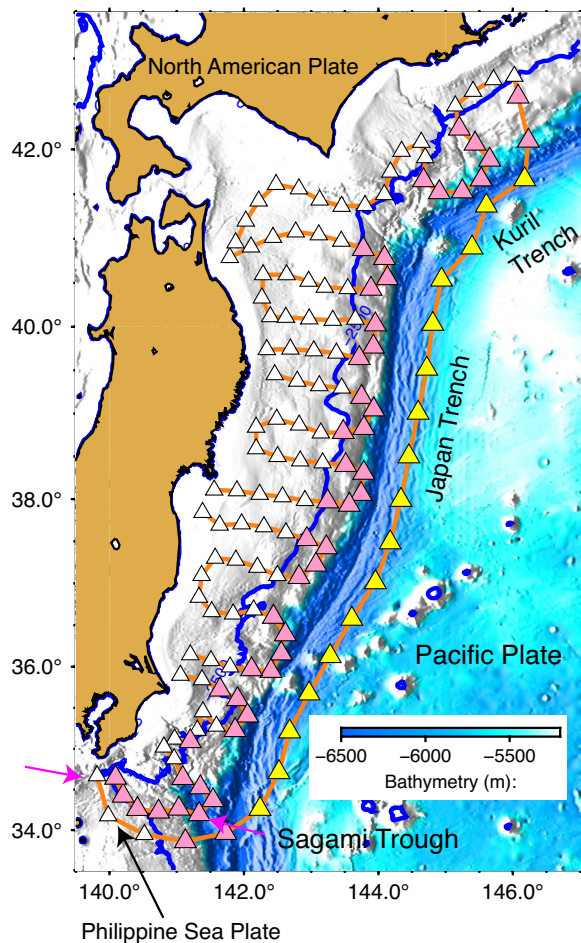


Fig. 1 Maps showing the locations of the S-net stations. Yellow triangles show the stations along the S6 cable which are located east of the Japan Trench; pink triangles represent the stations west of the Japan Trench and their water depths are deeper than 2,500 m. White triangles indicate the stations deployed < 2,500 m and not used in this study

stations deployed on the overlying plate west of the Japan Trench and 17 on the incoming oceanic plate east of the trench, mainly along the S6 cable. Each station comprises a velocity meter with a natural frequency of 15 Hz, and reliable noise spectra at frequencies > 0.2 Hz have been obtained in the S-net records (Takagi et al. 2021).

We used teleseismic events observed by the velocity meters for the receiver function analyses. The data are analyzed from September 2016 to January 2022. The three components of the XYZ coordinate for the S-net data, which are defined within the cable, are rotated to those of the RTV coordinates through the conversion to the ENV coordinate (Takagi et al. 2019), where R, T, V, E, and N are the radial, transverse, vertical, east, and north components, respectively. We collected teleseismic events with epicentral distances of 30°–90° and magnitudes of ≥ 5.5 , using the USGS Preliminary Determination of Epicenters (PDE) catalog (Sipkin et al. 2000). To calculate RFs, the information on the P-wave arrival times for the teleseismic events is required. We applied a bandpass filter of 0.5–2.0 Hz to the rotated waveforms to remove large noise levels of microseisms at lower frequencies than 0.5 Hz, and manually picked up the P-wave arrival times.

3 Methods

3.1 Receiver function analysis

The RFs, $RF(\omega)$, are calculated through the deconvolution of the horizontal component, $H(\omega)$, by the vertical component, $Z(\omega)$, with setting a water level (c) (Langston 1979), and are expressed as follows:

$$RF(\omega) = \frac{H(\omega)Z^*(\omega)}{\phi(\omega)}G(\omega), \quad (1)$$

where

$$\phi(\omega) = \max\{Z(\omega)Z^*(\omega), c \cdot \max\{Z(\omega), Z^*(\omega)\}\}, \quad (2)$$

$$G(\omega) = \exp\left(\frac{-(\omega - \omega_0)^2}{4\alpha^2}\right). \quad (3)$$

The water level setting in the denominator of Eq. (2) stabilizes the spectral division, and we selected $c=0.001$. $G(\omega)$ is the Gaussian filter, and we chose $\alpha=3.14$ and $f_0=2.0$ ($\omega_0=2\pi f_0$) and $f_0=1.5$ for stations west and east of the Japan Trench, respectively, which approximately results in bandpass filters of 1.0–3.0 Hz and 0.5–2.5 Hz. We used the relatively low frequency band for the incoming plate to detect P_s waves converted from the oceanic Moho, which is located deep at 6–7 km from the seafloor (Fig. 2). Because large amplitudes of microseisms are sometimes observed

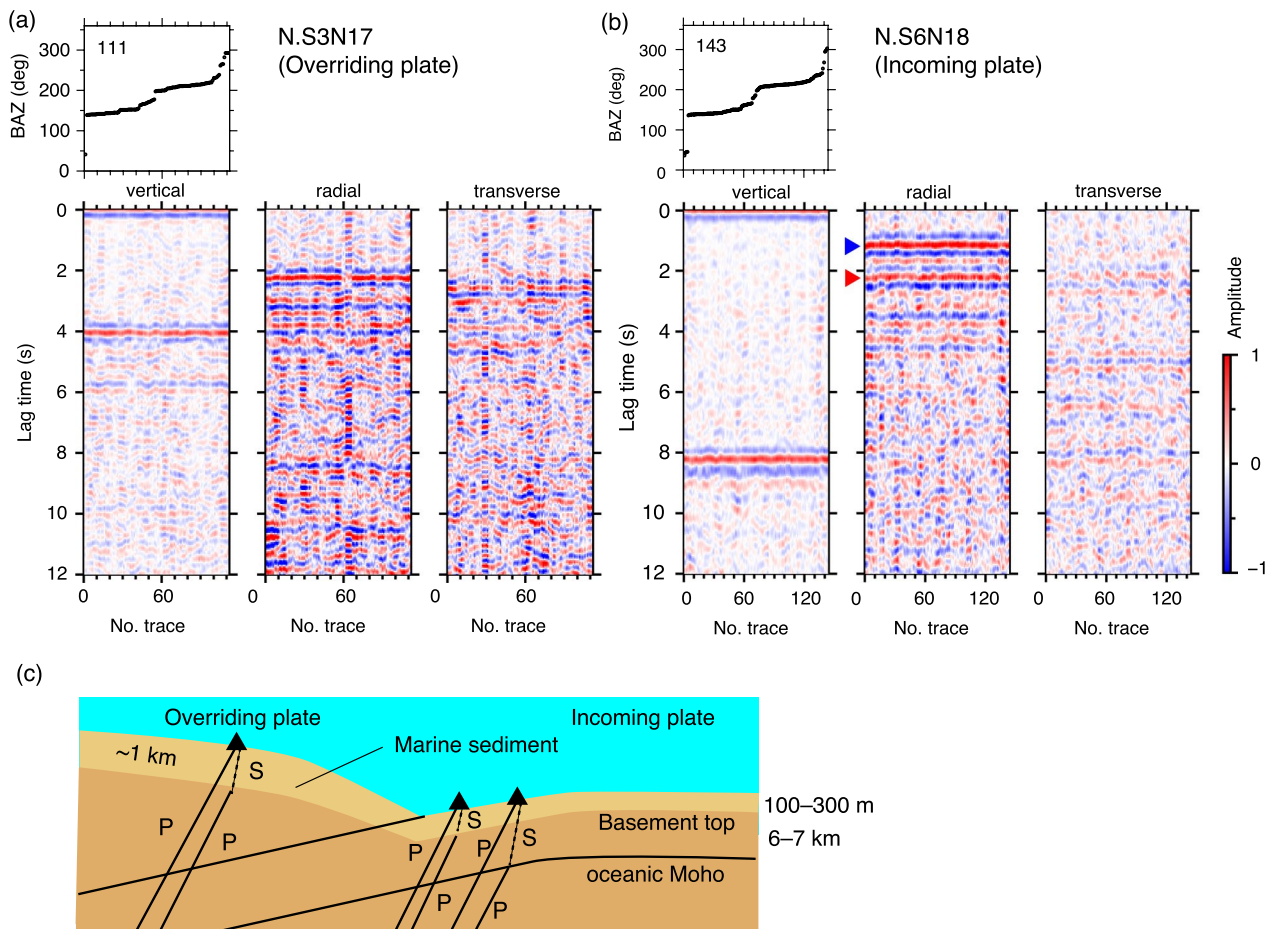


Fig. 2 RF waveforms and P-to-s converted waves. **a** The top panel shows the back azimuth (BAZ) of the used RFs for the station N.S3N17 at 1–3 Hz. The bottom three panels represent the vertical, radial, and transverse RFs aligned as a function BAZ. The blue triangle indicates Ps waves converted from the top of the basement. **b** Same as panel (a), but for station N.S6N18 at 0.5–2.5 Hz. The red triangle indicates Ps waves converted from the oceanic Moho. **c** Schematic for P-to-s waves converted at the basement top and oceanic Moho

at >0.5 Hz, high-frequency RFs are suitable for splitting measurements. However, Ps waves in the RFs at 1.0–3.0 Hz at a couple of stations in the incoming plate were unclear compared to those at 0.5–2.5 Hz. We therefore used higher frequency components only for the overriding plate.

The time windows of the vertical and horizontal components for the deconvolution are $-2-4$ s and $-2-20$ s from the hand-picked *P*-wave arrival time, respectively. When we cannot pick *P* arrival times due to large noise levels, we discarded the waveforms. *P*-wave arrivals are contaminated by *P* waves reflected at the sea surface. Because they arrive at a few seconds after the direct *P* waves for stations deployed at shallow water depths, and these amplitudes overlapped with the direct *P* waves, we chose stations with water depths deeper than 2,500 m to avoid the contamination of *P*-wave reflections in the deconvolution.

Figure 2 shows an example of the vertical, radial, and transverse RFs at the stations N.S3N17 (overriding plate) and N.S6N18 (incoming plate), which are aligned as a function of the back azimuth (BAZ). Here, the vertical RFs are calculated through the deconvolution of the vertical component with a time window of $-2-20$ s by the one with a time window of $-2-4$ s. As shown in Fig. 2b (incoming plate), the positive amplitudes at lag times of 1.5 s and 2.2 s in the radial RFs correspond to *P*-to-*s* (*Ps*) waves converted at the top of the basement (bottom of soft marine sediment) and the oceanic Moho, respectively, which are consistent with those of a previous study (Tonegawa et al. 2018). For example, in the case of $V_p=1.6$ km/s (Shinohara et al. 2008), $V_p/V_s=8$ (Fujie et al. 2013), and a sediment thickness of 300 m for a marine sediment layer (e.g., Fujiwara et al. 2007; Nakamura et al. 2023), the *Ps* time from the basement top results in 1.31 s for the vertical incident. In addition, for

$V_p=5.4$ km/s, $V_p/V_s=1.85$ (e.g., Fujie et al. 2013), and a crustal thickness of 6 km for an igneous crust underlying the marine sediment, the P_s time from the oceanic Moho through the sediment layer assumed above results in 2.25 s. Moreover, P_s waves at the lag time of 1.5 s may correspond to the top of the chert layer, which is hard siliceous sediments and substantially has a faster seismic velocity than that of overlying soft marine sediments (Fujie et al. 2020).

In contrast, as shown in Fig. 2a (overriding plate), the radial RFs for the overriding plate exhibit several coherent waves, and the first arrival (~ 2 s in lag time) corresponds to a P_s wave converted at the top of the basement. The thickness of the marine sediment layer is approximately 1 km (Tsuru et al. 2002). For example, in the case of $V_p=1.5$ km/s (Tsuru et al. 2002) and $V_p/V_s=4.4\text{--}5$ (e.g., Obana et al. 2019; Fukushima et al. 2022), the P_s time from the basement top results in 2.27–2.67 s. For the transverse RFs for those stations, small amplitudes are observed at lag times similar to P_s waves that emerged in the radial RFs, which indicate an anisotropic structure between the seafloor and the seismic interfaces that generate the P_s waves. In the vertical RFs, large amplitudes are observed at lag times of 8 s (N.S6N18) and 4 s (N.S3N17), respectively, which correspond to the first water reverberation of the P wave. Examples of the radial RFs at stations along S2, S3, and S6 cables are displayed in Fig. 3 and the other cables are shown in Fig. S2.

3.2 P_s splitting analysis

To obtain the anisotropic structure, we apply a traditional S-wave splitting analysis (Ando et al. 1980) to P_s converted waves in the radial and transverse RFs. Fast and slow polarization directions are present in an anisotropic medium. When S waves impinge on such anisotropic media, they separate into two S waves polarized into the fast and slow directions and propagate at different speeds. Since such a splitting also occurs in P_s converted waves propagating in an anisotropic medium, it is possible to estimate the fast/slow polarization direction and delay time between fast and slow S waves by applying S-wave splitting analysis to P_s converted waves.

We follow previous P_s splitting analyses for land cases (Nagaya et al. 2008, 2011) and an ocean case (Tonegawa et al. 2018). For the incoming Pacific Plate, we apply (I) the splitting analysis to P_s waves converted at the top of the basement, (II) the stripping technique to the radial and transverse RFs to remove the effects of the anisotropic structure shallower than the basement, including the delay time, from P_s waves converted at the oceanic Moho (Oda 2011), and (III) the splitting analysis of the processed P_s waves for the oceanic Moho. When P waves originate from the azimuth at which the fast/

slow axis of the sediment layer is oriented, S waves are not split, and then the delay time in step (I) becomes zero. Even in this case, we proceed to step (III) to estimate the anisotropic structure within the oceanic crust. These steps allow us to obtain anisotropic structures in each layer, that is, marine sediments and oceanic crust (Fig. 4). The anisotropic parameters obtained for the oceanic crust may include those of the chert layer when P_s waves are converted at the top of the chert layer. However, because the chert layer is typically thin (tens to hundreds of meters) and has a substantially high seismic velocity (e.g., Nakamura et al. 2013; Moore et al. 2015; Fujie et al. 2020; Qin et al. 2022), the effects of the chert layer on the estimated anisotropic parameters of the oceanic crust are considered to be small. The starting and ending times of the time window for the splitting measurement for all RFs observed at each station were unity, in which large P_s amplitudes in the radial and transverse RFs are included, and the time window length is 1 s (Fig. S3). Low-quality RFs with a periodic function due to the instability of the deconvolution are contaminated, and such RFs are manually excluded from the candidates for the splitting measurements (Fig. 3 and S3). For an overriding plate, we apply the splitting analysis to P_s waves converted at the top of the basement and obtain the anisotropic information for the soft marine sediments. The top of the basement within the overriding plate may dip slightly (e.g., Tsuru et al. 2002). According to the results from three-dimensional numerical simulations containing an anisotropic medium above a dipping interface (Tonegawa et al. 2017), the estimated fast polarization directions are slightly fluctuated as a function of BAZ, whereas the accurate delay times can be obtained by the splitting analysis.

This processing can be applied to a single teleseismic event. For a single event, we rotate the radial and transverse RFs in 1° increments and calculate the cross-correlation functions between the two rotated waveforms with a time window of 1 s. We search for the rotation angle and delay time for which the cross-correlation coefficient reaches a maximum. The search range of the rotation angle and delay time are $0\text{--}180^\circ$ and $0.0\text{--}0.1$ s with increments of 0.01 s, respectively. We did not use the event for the cross-correlation coefficient <0.9 or the delay time <0.01 s ($=0.00$ s). The fast polarization direction can be obtained using the BAZ information for a single event.

To display the obtained anisotropic structure, we count the number of the fast polarization directions with an azimuthal bin of 15° (rose diagram). The size of the rose diagram is normalized by its maximum number, and the delay time averaged over all of the available events is multiplied by the normalized size of the rose diagram. Rose

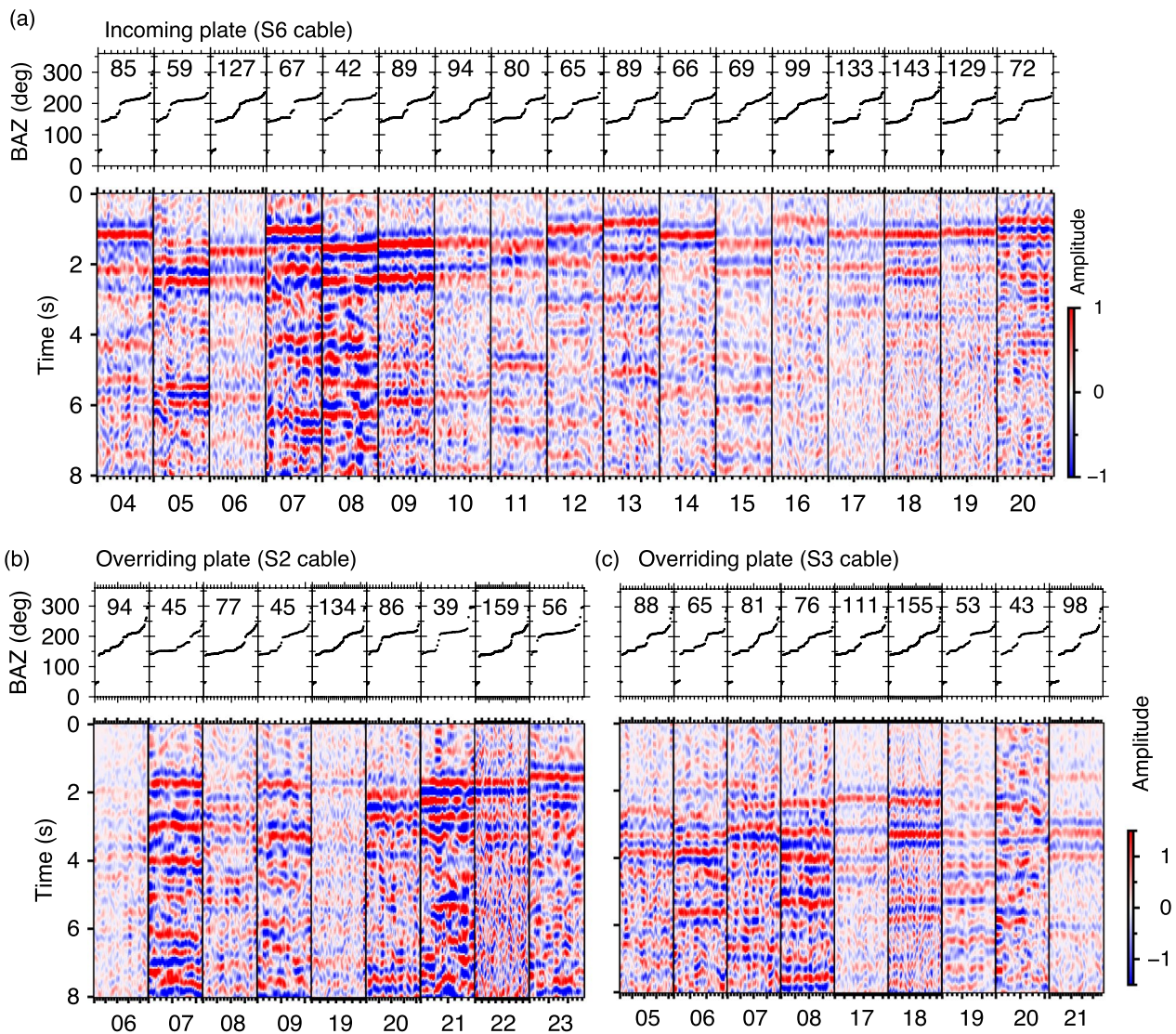


Fig. 3 Radial RF examples for **a** S6 cable (0.5–2.5 Hz), **b** S2 cable (1–3 Hz), and **c** S3 cable (1–3 Hz). The top panels represent the back azimuth (BAZ) of the used RFs, where the numbers of the used RFs are displayed. At the bottom, each panel shows the radial RFs as a function of BAZ for a single station. The bottom number indicates the station code for each cable (see Fig. S1)

diagrams are plotted at the station location, and the size of the rose diagram indicates the degree of the anisotropy beneath the station.

4 Results

For the incoming Pacific Plate, Ps waves converted from the basement top and oceanic Moho can be traced at stations along the S6 cable (Fig. 3a). The Ps signals used for the splitting measurements are indicated by boxes in Fig. S3. Several stations show three coherent positive signals with a weak second signal (e.g., N.S6N08, N.S6N09, and N.S6N13), and it appears that the weak second signal corresponds to Ps waves converted from

the bottom of the chert layer. We therefore used the first and third signals as Ps waves for the basement top (or the top of the chert layer) and oceanic Moho (Fig. 3a and S3). Especially, the lag time difference of the first Ps waves along the S6 cable indicates that the sediment thickness varies at short wavelengths, which is consistent with the results of an extensive seismic exploration survey (Nakamura et al. 2023). The amplitudes of the first Ps waves are comparable over most the stations. In contrast, the third Ps wave amplitudes are strong and weak at the northern (e.g., N.S6N04–N.S6N09) and southern stations (e.g., N.S6N14–N.S6N20), respectively (Fig. 3a). Fujie et al. (2023) suggested that the

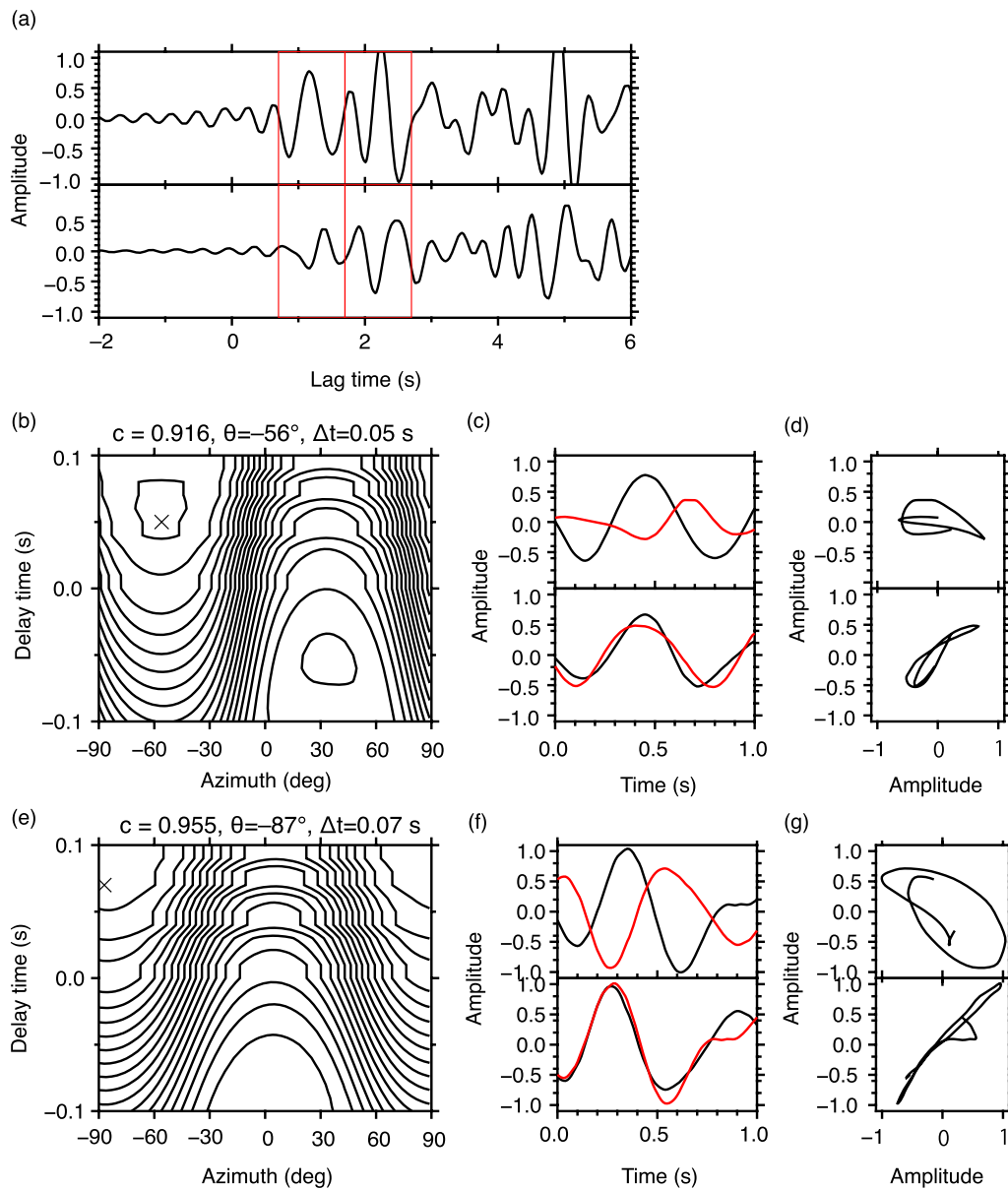


Fig. 4 Estimation of the anisotropic parameters. **a** Top and bottom waveforms correspond to the radial and transverse RFs. Left and right red boxes are the time windows in which Ps waves converted from the basement top and oceanic Moho are contained. **b** The distribution of cross-correlation coefficient as functions of the rotated azimuth and delay time for the Ps wave converted from the basement top. Estimated parameters c , θ , Δt are cross-correlation coefficient, rotated azimuth, and delay time. **c** The top panel shows waveforms of (black) radial and (red) transverse components, while the bottom shows the corrected waveforms. **d** Particle motions of panel (c). **e–f** Same as panels (b–d), but for Ps waves converted from the oceanic Moho

Hokkaido Rise is present in the outer-rise region along the Kuril Trench and the northern Japan Trench, and that structural changes are observed in the Hokkaido Rise: the Pacific Plate consists of marine sediments, oceanic crust, and oceanic lithosphere, and their thicknesses and seismic velocities are different between the Hokkaido Rise and other regions. In particular, the crustal thickness difference can be explained by

isostatic equilibrium to a certain degree (Fujie et al. 2023). The lateral variation in the Ps amplitudes for the oceanic Moho may be related to the structural difference. For the overriding plate (Fig. 3b, c and S2), the radial RFs at most stations exhibit the first Ps arrivals at lag times of 1–4 s, whereas those at some stations do not show coherent signals, for which we did not use the RFs for the anisotropy analyses.

The obtained fast polarization directions at the marine sediment in the incoming Pacific Plate are obliquely aligned to the trench axis at the northern stations; however, those at two stations, N.S6N04 and N.S6N11, show the directions parallel to the trench axis (region A in Fig. 5a). The fast polarization directions in the southern part are mainly parallel to the trench axis (region B in Fig. 5a). The degrees of the anisotropy are comparable across all of the stations. In igneous oceanic crust, the fast polarization directions tend to be aligned parallel to the trench axis. The degrees of the

anisotropy are almost comparable across the stations as well (Fig. 5b).

For the overriding plate west of the Japan Trench, in addition to the results of individual stations, we created rose diagrams in which (1) stations that show similar directions are grouped, and (2) the average delay times for the fast polarization directions over the stations in each group are summed at 15° bins. We divided the survey area into four regions (C–F) (Fig. 6). Measurements at a single station between regions E and F were not considered for the interpretation, because its pattern

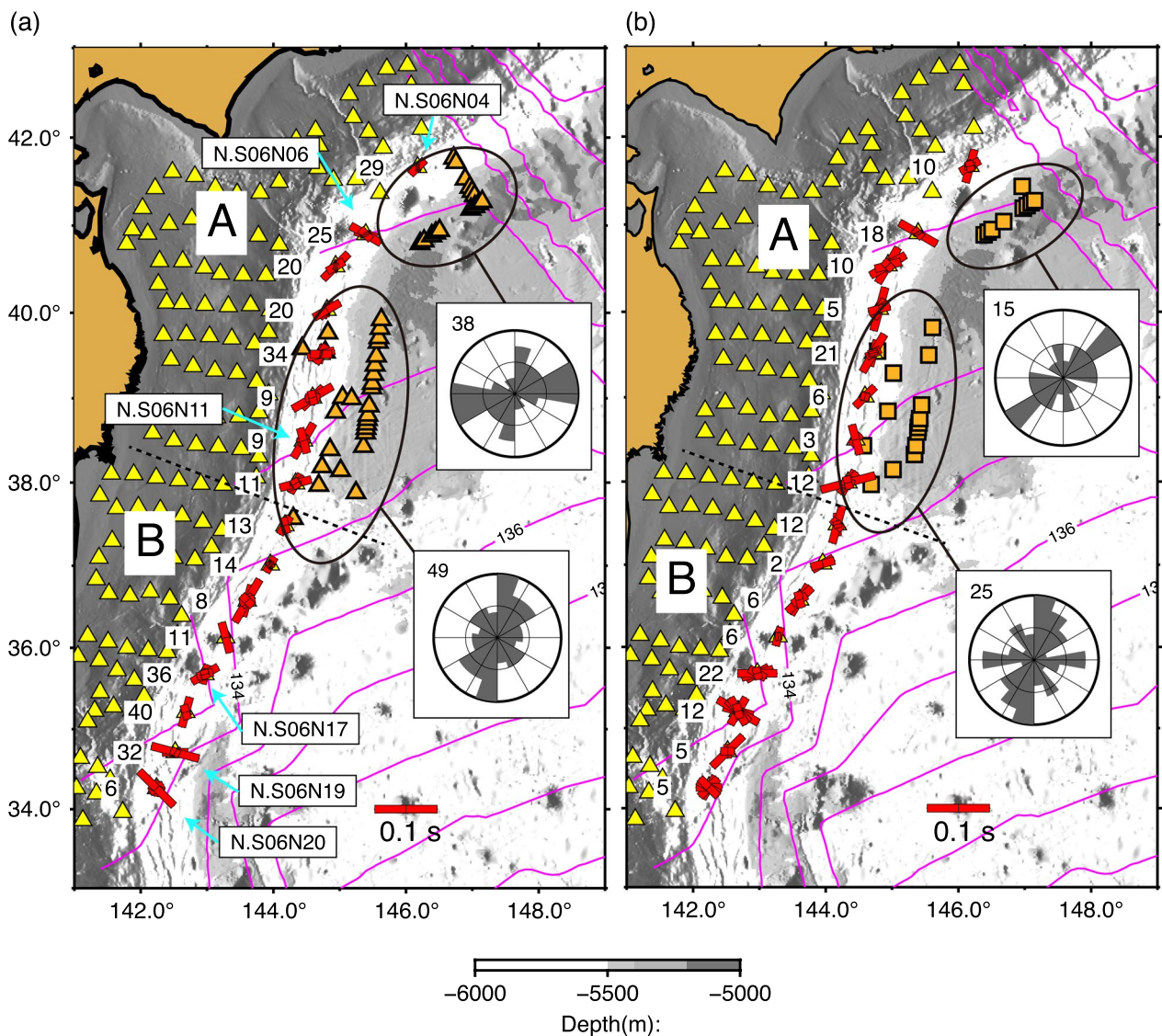


Fig. 5 The obtained fast polarization directions for **a** marine sediments and **b** igneous oceanic crust for the incoming Pacific Plate. Regions A and B are separated by dashed lines. Red bars indicate the rose diagrams of the fast polarization directions. The numbers left of the stations represent the numbers of the used RFs for the measurements. The rose diagrams in the insets and orange triangles show the results from Tonegawa et al. (2018) and the stations used in that study, with the number of events used for the measurements. Purple lines indicate the age of oceanic plates with an interval of 2 Ma (Müller et al. 2008)

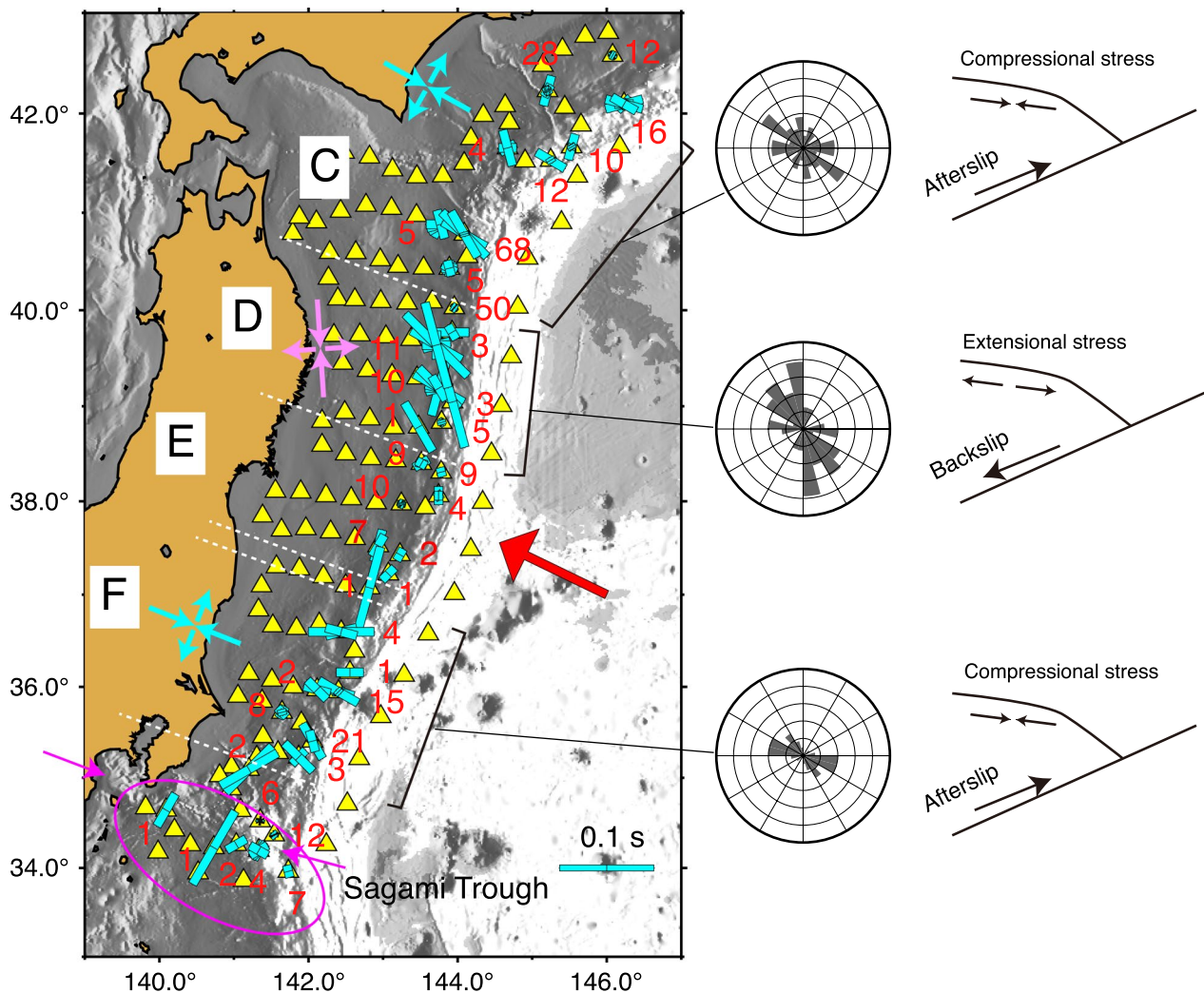


Fig. 6 The obtained fast polarization directions for marine sediments of the overlying plate west of the Japan Trench (light-blue bars). Red arrow represents the plate motion with a direction of N65°W (DeMets 1992). Rose diagrams on the right show the features for regions C, D, and F (see the text). The red-colored numbers indicate the RF numbers used for the measurements. Light-blue and pink arrows represent the stress fields inferred from the obtained anisotropic structure. The ellipse indicates the fast polarization directions estimated at the stations on the Philippine Sea Plate

is not consistent with those at surrounding stations. To investigate this local pattern in more details, it may be necessary to deploy temporary seismometers around this region. In regions C and F, the fast polarization directions are nearly normal to the trench axis (Fig. 6). However, the features of the anisotropic structures in between the two regions are different, and this area can be divided into two regions (D and E in Fig. 6). The fast polarization directions are aligned almost parallel to the trench axis in region D, whereas small degrees of the anisotropy are observed in region E.

5 Discussion

5.1 Incoming plate

To investigate the lateral variation in the fast polarization direction along the subduction direction in the incoming Pacific Plate, we compare our results with those of Tonegawa et al. (2015) (Fig. 5). The S-net stations east of the Japan Trench are mainly located in the region where the seafloor of the incoming plate slightly dips toward the trench, while the stations in the previous study are distant from the trench and are distributed in the flattened region or slightly upward-bended region due to the plate flexure (outer-rise region). Using the results from the two

datasets, we can investigate whether the anisotropy in the outer-rise region is preserved in the trench.

For the marine sediments, the fast polarization directions of the marine sediment in the outer-rise region are almost oriented parallel to the trench, whereas those east of the northern part of the trench are obliquely aligned to the trench axis (region A in Fig. 5a, b). The trench-parallel directions correspond to crack alignments that are created by the stress field applied to the marine sediments, and the stress field is induced by the plate bending in the outer-rise region: the extensional stress field normal to the trench axis and the compressional stress field parallel to the trench axis are created at the top part of the oceanic plate by the plate flexure in the outer-rise region. Such stresses also presumably induce normal faults with trench-parallel strike directions. In this case, because the fast polarization directions reflect the structural fabrics, that is, normal faults, the orientations of the fast directions are consistent with those of the stress-induced cracks.

Changes in the fast directions from parallel to oblique to the trench axis along the subduction direction indicate that cracks due to the plate bending are altered by those created from other factors. One possibility is the reactivation of ancient faults that were created when the Pacific Plate was formed at the spreading ridge. Nakanishi (2011) revealed that the strike directions of escarpments at the bathymetry at latitudes of 38°–39.5° N exhibit a north–south direction, parallel to the trench axis, and a northeast direction, which corresponds to the magnetic anomaly lineations for the Pacific Plate. Figure 5 also shows the contour lines of plate age (Müller et al. 2008), which indicates the strike direction of the ancient spreading ridge. When the plate was created at the spreading ridge, sufficient cracks parallel to the ridge direction were formed in the shallow part of the oceanic crust. Possibly, such cracks are reactivated due to the plate flexure before the subduction because they are weaker than the surrounding parts of the plate, and the displacement of the fault within the shallow oceanic crust may reach the overlying sediment.

In contrast, the fast polarization directions in the entire oceanic crust are aligned parallel to the trench axis from the outer-rise region to the trench. This is also caused by cracks and normal faults created by the stress field owing to the plate flexure. Extensional stresses are applied in the direction normal to the trench, and it appears that cracks and normal faults parallel to the trench axis are developed. Crustal minerals, including glaucophane, epidote, lawsonite, and phengite, have anisotropic seismic velocities. However, strong anisotropy is induced by crystal preferred orientations of these minerals under deformation, and such conditions occur within subducting slabs

(e.g., Bezacier et al. 2010; Cao et al. 2013; Kim et al. 2013; Ha et al. 2019; Lee et al. 2021; Park and Jung 2022). Anisotropic structures within the oceanic crust prior to subduction has been mainly detected near the ridge axis by seismic exploration surveys, and they are interpreted by the formation of cracks aligned with the ridge axis (e.g., Stephen 1985; Christeson et al. 2019). In the case of the Juan de Fuca Ridge, the degree of anisotropic structure tends to decrease away from the ridge due to infilling of cracks by mineral precipitation (Weekly et al. 2014). Seismic exploration surveys around a borehole station in the northwestern Pacific basin found isotropic P-wave velocities within the oceanic crust (layer 2 and layer 3) (Shinohara et al. 2008). Therefore, we consider that the obtained anisotropy within the oceanic crust near the Japan Trench is primarily attributed to newly created crack alignments.

Throughout the study region, there are some stations where the fast polarization directions for both the sediment and oceanic crust are oriented differently from those at nearby stations. Near these stations (e.g., N.S6N06, N.S6N17, N.S6N19, and N.S6N20), specific topographic anomalies, including seamounts, can be observed in the seafloor topography, indicating that volcanic activity occurred in the Pacific Plate in the past. The results obtained may have originated from such volcanic activities, including dike intrusions (Fujie et al. 2020), or/and the generation of cracks due to the loading of such seamounts applied to their internal and surrounding areas. Changes in stress-induced anisotropy due to the loading of volcanoes have also been observed in land (e.g., Johnson et al. 2011).

5.2 Overriding plate

We obtained fast polarization directions nearly normal to the trench axis in regions C and F. This indicates that cracks oriented in the direction are developed by the compressional stresses at shallow depths in the overriding plate (light-blue arrows in Fig. 6). In contrast, the fast polarization directions in region D in the central part are parallel to the trench axis. This result indicates that the compressional stresses parallel to the trench axis are applied to the overriding plate near the trench, and the extensional stresses normal to the trench are dominated (pink arrows in Fig. 6). The small degrees of the anisotropy in region E are caused by randomly distributed cracks, which are attributed to the small compressional and extensional stresses around this region.

The obtained fast polarization directions may reflect the stress field due to the postseismic deformation associated with the 2011 Tohoku-Oki earthquake. Regions D and E are near the large slip area of the 2011 Tohoku-Oki earthquake (e.g., Iinuma et al. 2012). Because we

do not have information on the anisotropy before 2016 due to the starting time of the S-net observation, it is unclear whether the stress field obtained in this study was created and/or affected by the 2011 Tohoku-Oki earthquake. However, postseismic crustal movements after the earthquake have been observed by seafloor geodetic observations using Global Navigation Satellite System (GNSS)–acoustic ranging combined with a seafloor positioning system (GNSS-A). Moreover, several studies found temporal changes in anisotropic structure at shallow depths after large earthquakes, e.g., the 1999 Chia-Yi earthquake, Taiwan (Chao and Peng 2009), the 2011 Tohoku-Oki earthquake, Japan (Nakata and Snieder 2012; Takagi and Okada 2012; Tonegawa et al. 2013), and the 2016 Kumamoto earthquake, Japan (Sawazaki et al. 2018).

Although the postseismic horizontal displacements on land mainly show trenchward movements (Ozawa et al. 2012), those near the Japan Trench using the GNSS-A are oriented landward at latitudes of 37°N–39.5° N (Watanabe et al. 2014; Tomita et al. 2017; Honsho et al. 2019) and trenchward south of 37° N (e.g., Tomita et al. 2017; Honsho et al. 2019; Dhar et al. 2022), which are related to the viscoelastic stress relaxation in the asthenosphere and the afterslips at the plate interface (Sun et al. 2014, 2015; Watanabe et al. 2014; Noda et al. 2018). The landward movements observed in the limited offshore area (37°N–39.5°N) have been continued at least until 2020, which are mainly controlled by the viscoelastic stress relaxation and interseismic backslip at the plate interface (Watanabe et al. 2021). Such interseismic backslip components may induce the extensional stresses in the direction normal to the trench at shallow depths of the overriding plate. The anisotropic structure in region D obtained in this study can be attributed to this extensional stress (Fig. 6). The trenchward movement south of 37°N may be caused by the spatial heterogeneity of the afterslip (Tomita et al. 2017). This afterslip induces the compressional stress at shallow depths in the overriding plate (Fig. 6). On the other hand, in region C, it may be difficult that the compressional stress is explained by the afterslip of the earthquake. Although the afterslips can promote slow earthquake activities, the observed slow earthquake activities in region C did not change substantially before and after the earthquake (Baba et al. 2020). One possibility would be afterslips due to the 2003 Tokachi-Oki earthquake (Mw 8.3). If the afterslips of the earthquake continues, the compressional stress in region C can be explained by the induced postseismic crustal deformation.

The reason for the low degree of the anisotropy in region E is unclear. However, it seems that along the direction normal to the trench in the large slip area, the

extensional stress had been created by interseismic backslip before the earthquake, the compressional stresses were dominant immediately after the earthquake, and then the stress field tends to be the extension due to the backslip. The small deviatoric stress in region E can be attributed to the temporal transition of the stress field from the compression to the extension. Otherwise, Kubota et al. (2022) suggested that, in the interseismic period before the 2011 Tohoku-Oki earthquake, shear stresses were not accumulated in the shallow part of the plate boundary around the large slip area. If similar situations occur after the earthquake in region E, the small deviatoric stresses can be explained by the less mechanical locking of the shallow plate boundary before and after the earthquake. Moreover, the degree of the anisotropy in region D appears to be large compared to those in regions C, E, and F. If the degrees of deviatoric stresses at the tip of the overriding plate are controlled by the coupling strength at the shallow plate interface, the lateral variations in the anisotropic intensity along the strike direction may reflect the heterogeneities of the plate coupling.

The stations in the southernmost part of the S-net are located on the Philippine Sea Plate (Figs. 1 and 6), and the fast polarization directions at the stations are mainly oriented in the NNE–SSW direction, which is normal to the Sagami Trough (ellipse in Fig. 6). This may indicate the compressional stress along the direction within the Philippine Sea Plate. However, because the numbers of the measurements are relatively small, it is necessary to collect more data to investigate this region in more details.

5.3 Anisotropic structure over the entire region of the overlying plate

Uchida et al. (2020) revealed that the fast directions are predominantly oriented parallel to the trench axis in the landward area of the S-net from the Kuril Trench to the Japan Trench, and interpreted that the trench-parallel directions are caused by normal faults within the overriding plate. Uchida et al. (2020) unveiled the anisotropic structures within the crust and western part of the S-net, whereas our results correspond to those in the shallowest part of the crust (sediment) and the tip of the overriding plate. However, combined with the results of Uchida et al. (2020), the trench-parallel fast directions are prevalent over the region D, and the trench-parallel fast directions on the landward sides in regions C and F shift to the trench-normal fast directions on the trenchward sides. Therefore, stress-induced cracks due to afterslips may be predominant at the tip of the overriding plate in regions C and E, compared with normal faults. In region D, stress-induced cracks due to backslips are oriented parallel to the trench, and normal faults with trench-parallel strike directions are also dominant. The fast

directions obtained in this region possibly correspond to both the cracks and normal faults. Moreover, the delay times of Uchida et al. (2020) are slightly larger than those in this study, indicating that an anisotropic structure is present even beneath the sediment layer. However, to state this, the fast directions must not change substantially over the crust.

6 Conclusions

We present lateral variations in the anisotropic structure of marine sediments within the overriding plate along a trench-parallel direction west of the Japan Trench. The fast polarization directions are possibly controlled by the stress fields associated with the postseismic crustal deformations of the 2011 Tohoku-Oki earthquake and maybe the 2003 Tokachi-Oki earthquake. We also obtained lateral variations in the fast polarization direction for the marine sediment and igneous oceanic crust within the incoming Pacific Plate east of the Japan Trench, which are affected by normal faults due to the plate flexure and partly by the reactivation of ancient faults. Therefore, the anisotropic structures of the overlying and incoming plates substantially reflect different factors.

Abbreviations

RF	Receiver function
S-net	Seafloor observation network for earthquakes and tsunamis along the Japan Trench
GNSS	Global Navigation Satellite System

Supplementary Information

The online version contains supplementary material available at <https://doi.org/10.1186/s40623-024-02059-8>.

Supplementary material 1.

Acknowledgements

The authors used the data of the S-net (NIED, 2019), operated by National Research Institute for Earth Science and Disaster Resilience.

Author contributions

T.T processed the data and drafted the manuscript. K.S and R.T suggested the approaches for analyses and expanded the contents of this study. T.T, K.S, and R.T contributed to the interpretation. All authors contributed to the final version of the manuscript.

Funding

This work was supported by JSPS KAKENHI Grant No. 18K03813, and No. JP21H05202 in Scientific Research on Transformative Research Areas "Science of Slow-to-Fast earthquakes."

Availability of data and materials

S-net data (NIED 2019) can be downloaded from the website operated by National Research Institute for Earth Science and Disaster Resilience (NIED) (<https://doi.org/https://doi.org/10.17598/NIED.0007>).

Declarations

Ethics approval and consent to participate

Not applicable.

Consent for publication

Not applicable.

Competing interests

The authors declare no competing interests.

Author details

¹Japan Agency for Marine-Earth Science and Technology (JAMSTEC), 3173-25, Showa-Machi, Kanazawa, Yokohama, Kanagawa 236-0001, Japan. ²National Research Institute for Earth Science and Disaster Resilience, 3-1, Tennodai, Tsukuba, Ibaraki 305-0006, Japan. ³Tohoku University, 6-6, Aza-Aoba, Aramaki, Aoba-Ku, Sendai 980-8578, Japan.

Received: 8 May 2024 Accepted: 16 August 2024

Published online: 30 August 2024

References

- Ammon CJ (1991) The isolation of receiver effects from teleseismic P waveforms. *Bull Seismol Soc Am* 81:2504–2510
- Ando M, Ishikawa Y, Wada H (1980) S-wave anisotropy in the upper mantle under a volcanic area in Japan. *Nature* 286:43–46. <https://doi.org/10.1038/286043a0>
- Aoi S, Asano Y, Kunugi T, Kimura T, Uehira K, Takahashi N, Ueda H, Shiomi K, Matsumoto T, Fujiwara H (2020) MOWLAS: NIED observation network for earthquake, tsunami and volcano. *Earth Planets Space* 72:126. <https://doi.org/10.1186/s40623-020-01250-x>
- Baba S, Takeo A, Obara K, Matsuzawa T, Maeda T (2020) Comprehensive detection of very low frequency earthquakes off the Hokkaido and Tohoku Pacific Coasts, Northeastern Japan. *J Geophys Res Solid Earth* 125:e2019JB017988. <https://doi.org/10.1029/2019JB017988>
- Bezacier L, Reynard B, Bass JD, Wang J, Mainprice D (2010) Elasticity of glaucophane, seismic velocities and anisotropy of the subducted oceanic crust. *Tectonophysics* 494:201–210. <https://doi.org/10.1016/j.tecto.2010.09.011>
- Cao Y, Jung H, Song S (2013) Petro-fabrics and seismic properties of blueschist and eclogite in the North Qilian suture zone, NW China: Implications for the low-velocity upper layer in subducting slab, trench-parallel seismic anisotropy, and eclogite detectability in the subduction zone. *J Geophys Res Solid Earth* 118:3037–3058. <https://doi.org/10.1002/jgrb.50212>
- Chao K, Peng Z (2009) Temporal changes of seismic velocity and anisotropy in the shallow crust induced by the 1999 October 22 *M* 6.4 Chia-Yi, Taiwan Earthquake. *Geophys J Int* 179:1800–1816. <https://doi.org/10.1111/j.1365-246X.2009.04384.x>
- Christeson GL, Goff JA, Reece RS (2019) Synthesis of oceanic crustal structure from two-dimensional seismic profiles. *Rev Geophys* 57:504–529. <https://doi.org/10.1029/2019RG000641>
- Crampin S (1977) A review of the effects of anisotropic layering on the propagation of seismic waves. *Geophys J Int* 49:9–27. <https://doi.org/10.1111/j.1365-246X.1977.tb03698.x>
- Crampin S (1981) A review of wave motion in anisotropic and cracked elastic-media. *Wave Motion* 3:343–391. [https://doi.org/10.1016/0165-2125\(81\)90026-3](https://doi.org/10.1016/0165-2125(81)90026-3)
- DeMets C (1992) Oblique convergence and deformation along the Kuril and Japan Trenches. *J Geophys Res* 97:17615–17625. <https://doi.org/10.1029/92JB01306>
- Dhakal YP, Kunugi T, Yamanaka H, Wakai A, Aoi S, Nishizawa A (2023) Estimation of source, path, and site factors of S waves recorded at the S-net sites in the Japan Trench area using the spectral inversion technique. *Earth Planets Space* 75:1. <https://doi.org/10.1186/s40623-022-01756-6>
- Dhar S, Muto J, Ito Y, Miura S, Moore JDP, Ohta Y, Iinuma T (2022) Along-arc heterogeneous rheology inferred from post-seismic deformation of the

- 2011 Tohoku-oki earthquake. *Geophys J Int* 230:202–215. <https://doi.org/10.1093/gji/ggac063>
- Dhar S, Muto J, Ohta Y, Iinuma T (2023) Heterogeneous rheology of Japan subduction zone revealed by postseismic deformation of the 2011 Tohoku-oki earthquake. *Prog Earth Planet Sci* 10:9. <https://doi.org/10.1186/s40645-023-00539-1>
- Fujie G, Kodaira S, Yamashita M, Sato T, Takahashi T, Takahashi N (2013) Systematic changes in the incoming plate structure at the Kuril trench. *Geophys Res Lett* 40:88–93. <https://doi.org/10.1029/2012GL054340>
- Fujie G, Kodaira S, Nakamura Y, Morgan JP, Dannowski A, Thorwart M, Greve-meyer I, Miura S (2020) Spatial variations of incoming sediments at the northeastern Japan arc and their implications for megathrust earthquakes. *Geology* 48:614–619. <https://doi.org/10.1130/G46757.1>
- Fujie G, Kodaira S, Obana K, Yamamoto Y, Isse T, Yamada T, No T, Nakamura Y, Miura S (2023) The nature of the Pacific plate as subduction inputs to the northeastern Japan arc and its implication for subduction zone processes. *Prog Earth Planet Sci* 10:50. <https://doi.org/10.1186/s40645-023-00578-8>
- Fujiwara T, Hirano N, Abe N, Takizawa K (2007) Subsurface structure of the “petit-spot” volcanoes on the northwestern Pacific Plate. *Geophys Res Lett* 34:L13305. <https://doi.org/10.1029/2007GL030439>
- Fukushima S, Shinohara M, Nishida K, Takeo A, Yamada T, Yomogida K (2022) Detailed S-wave velocity structure of sediment and crust off Sanriku, Japan by a new analysis method for distributed acoustic sensing data using a seafloor cable and seismic interferometry. *Earth Planets Space* 74:92. <https://doi.org/10.1186/s40623-022-01652-z>
- Ha Y, Jung H, Raymond LA (2019) Deformation fabrics of glaucophane schists and implications for seismic anisotropy: the importance of lattice preferred orientation of phengite. *Int Geol Rev* 61:720–737. <https://doi.org/10.1080/00206814.2018.1449142>
- Honsho C, Kido M, Tomita F, Uchida N (2019) Offshore Postseismic Deformation of the 2011 Tohoku earthquake revisited: application of an improved GPS-acoustic positioning method considering horizontal gradient of sound speed structure. *J Geophys Res Solid Earth* 124:5990–6009. <https://doi.org/10.1029/2018JB017135>
- Iinuma T, Hino R, Kido M, Inazu D, Osada Y, Ito Y, Ohzono M, Tsushima H, Suzuki S, Fujimoto H, Miura S (2012) Coseismic slip distribution of the 2011 off the Pacific Coast of Tohoku Earthquake (M9.0) refined by means of seafloor geodetic data. *J Geophys Res* 117:2012JB009186. <https://doi.org/10.1029/2012JB009186>
- Ito Y, Tsuji T, Osada Y, Kido M, Inazu D, Hayashi Y, Tsushima H, Hino R, Fujimoto H (2011) Frontal wedge deformation near the source region of the 2011 Tohoku-Oki earthquake. *Geophys Res Lett* 38:L00G05. <https://doi.org/10.1029/2011GL048355>
- Johnson JH, Savage MK, Townend J (2011) Distinguishing between stress-induced and structural anisotropy at Mount Ruapehu volcano, New Zealand. *J Geophys Res* 116:B12303. <https://doi.org/10.1029/2011JB008308>
- Kim D, Katayama I, Michibayashi K, Tsujimori T (2013) Deformation fabrics of natural blueschists and implications for seismic anisotropy in subducting oceanic crust. *Phys Earth Planet Int* 222:8–21. <https://doi.org/10.1016/j.pepi.2013.06.011>
- Kim H, Kawakatsu H, Akuhara T, Shinohara M, Shiobara H, Sugioka H, Takagi R (2021) Receiver function imaging of the amphibious NE Japan Subduction Zone—effects of low-velocity sediment layer. *J Geophys Res Solid Earth* 126:e2021JB021918. <https://doi.org/10.1029/2021JB021918>
- Kubota T, Saito T, Hino R (2022) A new mechanical perspective on a shallow megathrust near-trench slip from the high-resolution fault model of the 2011 Tohoku-Oki earthquake. *Prog Earth Planet Sci* 9:68. <https://doi.org/10.1186/s40645-022-00524-0>
- Langston CA (1979) Structure under Mount Rainier, Washington, inferred from teleseismic body waves. *J Geophys Res* 84:4749–4762. <https://doi.org/10.1029/JB084iB09p04749>
- Lee J, Mookherjee M, Kim T, Jung H, Klemd R (2021) Seismic anisotropy in subduction zones: evaluating the role of chloritoid. *Front Earth Sci* 9:644958. <https://doi.org/10.3389/feart.2021.644958>
- Moore JC, Plank TA, Chester FM, Polissar PJ, Savage HM (2015) Sediment provenance and controls on slip propagation: Lessons learned from the 2011 Tohoku and other great earthquakes of the subducting northwest Pacific plate. *Geosphere* 11:533–541. <https://doi.org/10.1130/GES01099.1>
- Müller RD, Sdrolias M, Gaina C, Roest WR (2008) Age, spreading rates, and spreading asymmetry of the world’s ocean crust. *Geochem Geophys Geosyst* 9:2007GC001743. <https://doi.org/10.1029/2007GC001743>
- Nagaya M, Oda H, Akazawa H, Ishise M (2008) Receiver functions of seismic waves in layered anisotropic media: application to the estimate of seismic anisotropy. *Bull Seismol Soc Am* 98:2990–3006. <https://doi.org/10.1785/B0120080130>
- Nagaya M, Oda H, Kamimoto T (2011) Regional variation in shear-wave polarization anisotropy of the crust in southwest Japan as estimated by splitting analysis of Ps-converted waves on receiver functions. *Phys Earth Planet Int* 187:56–65. <https://doi.org/10.1016/j.pepi.2011.04.016>
- Nakamura Y, Kodaira S, Miura S, Regalla C, Takahashi N (2013) High-resolution seismic imaging in the Japan Trench axis area off Miyagi, northeastern Japan. *Geophys Res Lett* 40:1713–1718. <https://doi.org/10.1002/grl.50364>
- Nakamura Y, Kodaira S, Fujie G, Yamashita M, Obana K, Miura S (2023) Incoming plate structure at the Japan Trench subduction zone revealed in densely spaced reflection seismic profiles. *Prog Earth Planet Sci* 10:45. <https://doi.org/10.1186/s40645-023-00579-7>
- Nakanishi M (2011) Bending-related topographic structures of the subducting plate in the Northwestern Pacific Ocean. In: Ogawa Y, Anma R, Dilek Y (eds) *Accretionary prisms and convergent margin tectonics in the Northwest Pacific Basin*. Springer, Dordrecht, pp 1–38
- Nakata N, Sneider R (2012) Time-lapse change in anisotropy in Japan’s near surface after the 2011 Tohoku-Oki earthquake. *Geophys Res Lett* 39:2012GL051979. <https://doi.org/10.1029/2012GL051979>
- NIED (2019) NIED S-net, National Research Institute for Earth Science and Disaster Resilience. <https://doi.org/10.17598/NIED.0007>
- Noda A, Takahama T, Kawasato T, Matsu’ura M (2018) Interpretation of offshore crustal movements following the 2011 Tohoku-Oki earthquake by the combined effect of afterslip and viscoelastic stress relaxation. *Pure Appl Geophys* 175:559–572. <https://doi.org/10.1007/s00024-017-1682-z>
- Obana K, Fujie G, Takahashi T, Yamamoto Y, Tonegawa T, Miura S, Kodaira S (2019) Seismic velocity structure and its implications for oceanic mantle hydration in the trench–outer rise of the Japan Trench. *Geophys J Int* 217:1629–1642. <https://doi.org/10.1093/gji/ggz099>
- Oda H (2011) Stripping analysis of Ps-converted wave polarization anisotropy. *Bull Seism Soc Am* 101:2810–2818. <https://doi.org/10.1785/B0120100323>
- Ozawa S, Nishimura T, Munekane H, Suito H, Kobayashi T, Tobita M, Imakiire T (2012) Preceding, coseismic, and postseismic slips of the 2011 Tohoku earthquake, Japan. *J Geophys Res* 117:2011JB009120. <https://doi.org/10.1029/2011JB009120>
- Park Y, Jung H (2022) Seismic velocity and anisotropy of glaucophane and epidote in experimentally deformed epidote blueschist and implications for seismic properties in warm subduction zones. *Earth Planet Sci Lett* 598:117822. <https://doi.org/10.1016/j.epsl.2022.117822>
- Qin Y, Nakamura Y, Kodaira S, Fujie G (2022) Seismic imaging of subsurface structural variations along the Japan trench south of the 2011 Tohoku earthquake rupture zone. *Earth Planet Sci Lett* 594:117707. <https://doi.org/10.1016/j.epsl.2022.117707>
- Sawazaki K, Nakamura T (2020) “N”-shaped Y/X coda spectral ratio observed for in-line-type OBS networks; S-net and ETMC: interpretation based on natural vibration of pressure vessel. *Earth Planets Space* 72:130. <https://doi.org/10.1186/s40623-020-01255-6>
- Sawazaki K, Saito T, Shiomi K (2018) Shallow temporal changes in S wave velocity and polarization anisotropy associated with the 2016 Kumamoto earthquake sequence, Japan. *J Geophys Res Solid Earth* 123:9899–9913. <https://doi.org/10.1029/2018JB016261>
- Shibazaki B (2023) Progress in modeling the Tohoku-oki megathrust earthquake cycle and associated crustal deformation processes. *Prog Earth Planet Sci* 10:43. <https://doi.org/10.1186/s40645-023-00575-x>
- Shinohara M, Fukano T, Kanazawa T, Araki E, Suyehiro K, Mochizuki M, Nakahigashi K, Yamada T, Mochizuki K (2008) Upper mantle and crustal seismic structure beneath the Northwestern Pacific Basin using a seafloor borehole broadband seismometer and ocean bottom seismometers. *Phys Earth Planet Int* 170:95–106. <https://doi.org/10.1016/j.pepi.2008.07.039>
- Sipkin SA, Persion WJ, Presgrave BW (2000) *Earthquake Bulletins and catalogs at the USGS National Earthquake Information Center*. IRIS Newslett 2000(1):2–4
- Stephen RA (1985) Seismic anisotropy in the upper oceanic crust. *J Geophys Res* 90:11383–11396. <https://doi.org/10.1029/JB090iB13p11383>

- Sun T, Wang K (2015) Viscoelastic relaxation following subduction earthquakes and its effects on afterslip determination. *JGR Solid Earth* 120:1329–1344. <https://doi.org/10.1002/2014JB011707>
- Sun T, Wang K, Iinuma T, Hino R, He J, Fujimoto H, Kido M, Osada Y, Miura S, Ohta Y, Hu Y (2014) Prevalence of viscoelastic relaxation after the 2011 Tohoku-oki earthquake. *Nature* 514:84–87. <https://doi.org/10.1038/nature13778>
- Takagi R, Okada T (2012) Temporal change in shear velocity and polarization anisotropy related to the 2011 M9.0 Tohoku-Oki earthquake examined using KIK-net vertical array data. *Geophys Res Lett* 39:2012GL051342. <https://doi.org/10.1029/2012GL051342>
- Takagi R, Uchida N, Nakayama T, Azuma R, Ishigami A, Okada T, Nakamura T, Shiomi K (2019) Estimation of the orientations of the S-net cabled ocean-bottom sensors. *Seis Res Lett* 90:2175–2187. <https://doi.org/10.1785/0220190093>
- Takagi R, Toyokuni G, Chikasada N (2021) Ambient noise correlation analysis of S-net records: extracting surface wave signals below instrument noise levels. *Geophys J Int* 224:1640–1657. <https://doi.org/10.1093/gji/ggaa548>
- Tomita F, Kido M, Ohta Y, Iinuma T, Hino R (2017) Along-trench variation in seafloor displacements after the 2011 Tohoku earthquake. *Sci Adv* 3:e1700113. <https://doi.org/10.1126/sciadv.1700113>
- Tonegawa T, Fukao Y, Nishida K, Sugioka H, Ito A (2013) A temporal change of shear wave anisotropy within the marine sedimentary layer associated with the 2011 Tohoku-Oki earthquake. *J Geophys Res Solid Earth* 118:607–615. <https://doi.org/10.1002/jgrb.50074>
- Tonegawa T, Fukao Y, Fujie G, Takemura S, Takahashi T, Kodaira S (2015) Geographical distribution of shear wave anisotropy within marine sediments in the northwestern Pacific. *Prog Earth Planet Sci* 2:27. <https://doi.org/10.1186/s40645-015-0057-2>
- Tonegawa T, Obana K, Yamamoto Y, Kodaira S, Wang K, Riedel M, Kao H, Spence G (2017) Fracture alignments in marine sediments off Vancouver island from Ps splitting analysis. *Bull Seismol Soc Am* 107:387–402. <https://doi.org/10.1785/0120160090>
- Tonegawa T, Obana K, Fujie G, Kodaira S (2018) Lateral variation of the uppermost oceanic plate in the outer-rise region of the Northwest Pacific Ocean inferred from Po-to-s converted waves. *Earth Planet Space* 70:106. <https://doi.org/10.1186/s40623-018-0880-y>
- Tonegawa T, Takagi R, Sawazaki K, Shiomi K (2023) Short-term and long-term variations in seismic velocity at shallow depths of the overriding plate west of the Japan trench. *J Geophys Res Solid Earth* 128:e2022JB025262. <https://doi.org/10.1029/2022JB025262>
- Tsuru T, Park J-O, Miura S, Kodaira S, Kido Y, Hayashi T (2002) Along-arc structural variation of the plate boundary at the Japan Trench margin: implication of interplate coupling. *J Geophys Res* 107(B12):2357. <https://doi.org/10.1029/2001JB001664>
- Uchida N, Nakajima J, Wang K, Takagi R, Yoshida K, Nakayama T, Hino R, Okada T, Asano Y (2020) Stagnant forearc mantle wedge inferred from mapping of shear-wave anisotropy using S-net seafloor seismometers. *Nat Commun* 11:5676. <https://doi.org/10.1038/s41467-020-19541-y>
- Watanabe S, Sato M, Fujita M, Ishikawa T, Yokota Y, Ujihara N, Asada A (2014) Evidence of viscoelastic deformation following the 2011 Tohoku-Oki earthquake revealed from seafloor geodetic observation. *Geophys Res Lett* 41:5789–5796. <https://doi.org/10.1002/2014GL061134>
- Watanabe S, Ishikawa T, Nakamura Y, Yokota Y (2021) Co- and postseismic slip behaviors extracted from decadal seafloor geodesy after the 2011 Tohoku-oki earthquake. *Earth Planets Space* 73:162. <https://doi.org/10.1186/s40623-021-01487-0>
- Weekly RT, Wilcock WSD, Toomey DR, Hooft EEE, Eunyong K (2014) Upper crustal seismic structure of the Endeavour segment, Juan de Fuca Ridge from traveltimes tomography: Implications for oceanic crustal accretion. *Geochem Geophys Geosyst* 15:1296–1315. <https://doi.org/10.1002/2013GC005159>

Publisher's Note

Springer Nature remains neutral with regard to jurisdictional claims in published maps and institutional affiliations.